Biotechnology Reports 24 (2019) xxx–xxx

Contents lists available at ScienceDirect

Biotechnology Reports

journal homepage: www.elsevier.com/locate/btre

Synthesis, characterization and biological activities of monometallic and bimetallic nanoparticles using *Mirabilis jalapa* leaf extract

Sumbal[a], Asifa Nadeem[a], Sania Naz[a], Joham Sarfraz Ali[a], Abdul Mannan[b], Muhammad Zia[a,*]

[a] Department of Biotechnology Quaid-i-Azam, University Islamabad, Pakistan
[b] Department of Pharmacy, COMSATS University, Abbottabad, Pakistan

ARTICLE INFO

Article history:
Received 6 March 2019
Received in revised form 5 April 2019
Accepted 7 April 2019

Keywords:
M. jalapa monometallic
Bimetallic
Biological properties
Nanoparticles

ABSTRACT

Monometallic ZnO and Ag nanoparticles (NPs) and bimetallic ZnO/Ag NPs were synthesized using leaves extract of *Mirabilis jalapa*. XRD analysis confirmed the crystalline nature of NPs with size range from 19.3 to 67.4 nm for bimetallic, and 12.9 and 32.8 nm for monometallic NPs. SEM images reveal varying shapes of the monometallic (needle like and spherical for ZnO and Ag, respectively) and bimetallic (plates, sheets, and spherical) NPs depending upon concentration of salts used. Biological characterization reveals that both mono and bi metallic nanoparticles demonstrate free radical scavenging, total antioxidant, and reducing power potentials. Phenolic and flavonoid like properties of NPs were also observed might be due to presence of different functional groups on the particles surface. Bimetallic NPs displayed astonishing antibacterial (up to 25 mm zone of inhibition) and antileishmanial properties. The results suggest that bimetallic ZnO/Ag nanoparticles hold greater potential then monometallic against bacteria and Leishmania. Other biomedical applications also varied depending upon concentration of precursors. Furthermore, ratio of salt concentrations used for synthesis of bimetallic NPs affect morphological and biochemical characteristics of NPs.

1. Introduction

The research in nanotechnology pledges quantum leaps not only in materials manufacturing and nanoelectronics but also possesses a lot of applications in healthcare, medicine, energy, biotechnology and safety. The unique properties displayed by nanoparticles are due to the increase in surface to volume ratio which alters the mechanical, thermal and catalytic properties of nanomaterial. The use of plant, algae, fungi, and bacteria provides ecofriendly, safe, reliable, and economical route to synthesize nanoparticles (NPs).

Metallic nanoparticles are categorized as monometallic, bimetallic, trimetallic, and so on depending on the number of metallic ingredients. For the preparation of bimetallic nanoparticles from precursor salts two methods are adopted: 1) Co-reduction; and 2) Successive reduction [1]. Though a number of bimetallic NPs have been synthesized through these processes but Ag and Zn are less investigated although both are considered as “biocidal agents” at independent level. ZnO NPs has proved effective against pathogens when used in minute quantities. In the context of monometallic ZnO NPs, their easy fabrication, environment affable nature and the non-toxic means of synthesis makes ZnO nanoparticles best alternative for a number of biological uses. ZnO NPs are used in solar cells, photo catalytic activities, photoluminescence, sensors, anticancerous properties [2]. They also possess antibacterial activity against broad spectrum microbes [3] and also have capability to absorb UV radiations, microwaves, infrared and radiofrequencies which enables them to be used in ointments and cosmetic creams [4]. Ag NPs display exclusive electrical and optical properties and can be used in surgical, food handling, packaging and storage tools, water purifiers, textiles, cosmetics, contact lenses, wound care products, implantable devices. Ag NPs also exhibit the most efficient antibacterial and antifungal properties [5]. The applications of both ZnO and Ag NPs validate the importance of both types of nanoparticles and require further exploration for the well-being of humans. Synthesis of ZnO/Ag bimetallic NPs has been performed via chemical and physical routes i.e. reduction by hydrazine hydrate [6]; solvothermal method [7]; ultrasonic irradiation [8]. However synthesis of bimetallic NPs through biogenic approach is lacking. So synthesis of ZnO/Ag bimetallic NPs via green synthesis i.e. utilization of *M. jalapa* leaf extract as the reducing agent for bioreduction of Zinc acetate and Silver nitrate into ZnO/Ag nanoparticles was designed.

* Corresponding author.
E-mail addresses: ziachaudhary@gmail.com, m.zia@qau.edu.pk (M. Zia).

https://doi.org/10.1016/j.btre.2019.e00338

In this study, synthesis and characterization of monometallic and bimetallic nanoparticles was performed using *M. jalapa* leaves extract to reduce zinc acetate and silver nitrate into nanoparticles. Furthermore, synthesized NPs were assessed for a series of biological assays i.e. Antimicrobial assays (Antibacterial and Antileishmanial), phytochemical assays (PLP, FLP) and Biological evaluation (DPPH Free radical Scavenging Assay, TRP and TAC). The study explores new insight into applications and combinatorial effect of zinc and silver in nanoparticle configuration.

2. Materials and methods

2.1. Preparation of aqueous leaf extract of M. jalapa

Fresh plant of Four O'clock (*Mirabilis jalapa* Linn) was collected from local areas of Rawalpindi, Pakistan and authenticated by Taxonomist Department of Plant Sciences, Quaid-i-Azam University, Islamabad. For preparation of leaf extract, the leaves were thoroughly washed with distilled water to get rid of dust particles and shade dried. The leaves were powdered in an electrical grinder and 10 g of the powder was soaked in 100 ml distilled water. After 24 h, the mixture was heated at $40 \pm 5\,^{\circ}C$ for 2 h with constant stirring. The contents were filtered through muslin cloth and Whatman filter paper. The extract was used for synthesis of nanoparticles.

2.2. Synthesis of monometallic and bimetallic nanoparticles

The precursor salts used for the synthesis of silver and zinc nanoparticles were silver nitrate ($AgNO_3$) and Zinc acetate ($Zn(O_2CCH_3)_2(H_2O)_2$). For synthesis of silver nanoparticles, 50 ml of extract was reacted with 0.5 M $AgNO_3$ under constant stirring at room temperature for reduction of Ag^+ ions to nanoparticles. Similarly, 50 ml leaf extract was also treated with 0.5 M Zinc acetate solution to form ZnO nanoparticles. ZnO-Ag Bimetallic nanoparticles were synthesized at five different molarities that were 0.5:0.5; 0.1:0.1; 0.5:0.1; 0.1:0.5; and 1:1 for Zinc acetate and Silver Nitrate, respectively. For each set, 50 ml of Four O'clock leaf extract was used as the reducing agent for 50 ml of salt solution. For synthesis of NPs, the extract was heated up to $60 \pm 5\,^{\circ}C$ upon constant stirring and Zinc acetate was added. After 5 min Silver nitrate solution was also added to the mixture and reaction was carried out for 2 h.

The synthesized nanoparticles were centrifuged at 13,000 rpm for 12 min and washed thrice with distilled water. The pellets were then dried and finely grinded in pestle and mortar for characterization and biological activities.

2.3. Characterization of nanoparticles

The crystalline structure of nanoparticles was characterized through X-Ray diffraction patterns by X-Ray Diffractometer (X'Pert pro of PAN Analytical Company) at a scanning rate of 2 θ angles/min at 40 kV and 30 mA current. The scanning range was kept between 10° and 80° using Nickel monochromatic Cu Kα radiation (θ = 1.5406 Å), NaI detector, variable slits and 0.02 scan step size. The crystallite size (D) was calculated using the Debye–Scherrer equation:

$$D = (k\lambda)/(\beta\cos\theta)$$

Where k is the proportionality constant (k = 0.9); λ is the X-ray wavelength coming from Cu-Kα; β is the full width at half maximum (FWHM) of the diffraction peak in radians; θ is the Braggs' angle in degree.

Scanning electron microscopy (SEM) was performed for morphological characterization and energy dispersive spectroscopy (EDS) for analysis of Elemental composition of metal Nanoparticles. For Scanning electron microscopy and EDS Philips XL 30 was used. This system provides both secondary electron and backscattered electron imaging with integrated EDAX system. Resolution of system was 3.5 nm @ 30 kV. Nicolet™ iS™ 5.

Fourier transform infrared spectroscopy (FTIR) for characterizing the surface chemistry and organic functional groups. System (Bruker FTIR) was equipped with Thermo Scientific™ OMNIC™ software, 100–240 V 50/60 Hz Power supply, and Fast recovery deuterated triglycine sulfate (DTGS) (standard) Detector. FTIR was done within spectral range of 3500 cm^{-1} - 500 cm^{-1} and Peak values of FTIR were finally compared with standard database.

2.4. Estimation of phenolic like property (PLP)

The estimation of phenolic like property of NPs was ascertained by Folin-Ciocalteu method utilizing Gallic acid as Positive control following the protocol reported by Javed et al, [9] with little alteration. A fraction of 20 μl from 4 mg/ml in DMSO was reacted with 90 μl of the Folin–Ciocalteu reagent in 96 well plate. After 5 min 90 μl Sodium carbonate was poured in each well and absorbance was recorded by microplate reader (Biotech USA, micro plate reader Elx 800) at 630 nm. The calibration curve ($y = 0.138x + 0.360$, $R^2 = 0.992$) was drawn in accordance with the absorbance of positive control i.e. Gallic acid at final concentrations of (25, 20, 15 and 10 μg/ml), under same operating conditions. The results are expressed as μg Gallic acid equivalent per milligram sample (μg GAE/mg sample).

Table 1
Summary of synthesis and Characteristics of Monometallic ZnO and Ag Nanoparticles and Bimetallic ZnO/Ag Nanoparticles.

SAMPLE	COLOR CHANGES	SIZE (nm)	SHAPE
0.5 M Zinc acetate	Slightly brown upon addition of Zinc acetate Dark brown Slightly rusty	12.9	Needle like structures
0.5 M Silver nitrate	Tea color upon addition of Silver nitrate Dark brown Blackish brown	32.8	Spherical
0.5 M Zinc acetate; 0.5 Silver nitrate	Slightly dark brown upon addition of Zinc acetate Brick brown upon addition of Silver nitrate Blackish brown	19.3	Plate like structures
0.1 M Zinc acetate; 0.1 M silver nitrate	Slightly dark brown upon addition of Zinc acetate Tea color upon addition of Silver nitrate Slight darkness in color Dark brown	30.3	Spherical
0.5 M Zinc acetate; 0.1 M Silver nitrate	Slightly dark brown upon addition of Zinc acetate Slight lightness in color upon addition of Silver nitrate Brown color	21.4	Spherical
0.1 M Zinc acetate; 0.5 M Silver nitrate	Slightly dark brown upon addition of Zinc acetate Tea color upon addition of Silver nitrate More lightness in color	15.2	Spherical
1 M Zinc acetate; 1 M Silver nitrate	Slightly dark brown upon addition of Zinc acetate Blackish silver upon addition of Silver nitrate Grayish silver with the passage of time	67.4	Sheet like structures

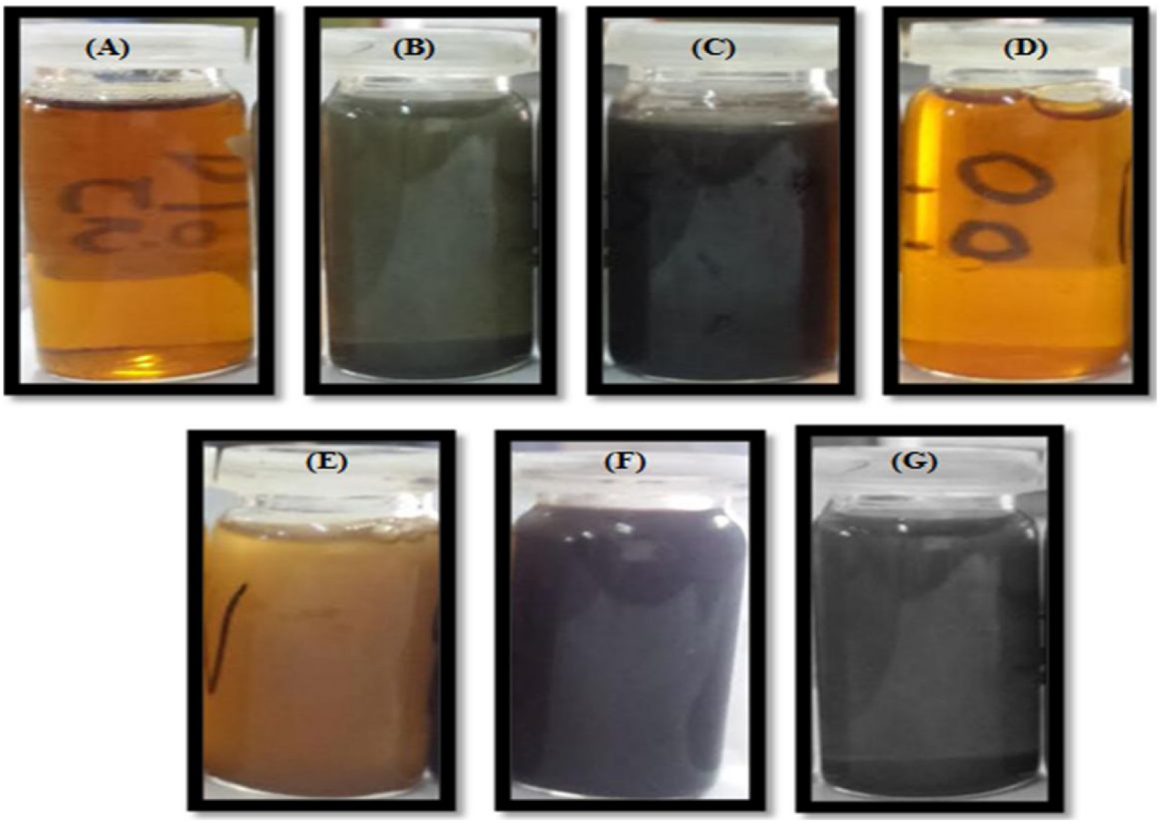

Fig. 1. Final colors of each reaction mixture after completion of the 2 h reaction (A) ZnO monometallic 0.5 M (B) Ag monometallic 0.5 M (C) ZnO/Ag bimetallic 0.5 M, 0.5 M (D) ZnO/Ag bimetallic 0.1 M, 0.1 M (E) ZnO/Ag bimetallic 0.5 M, 0.1 M (F) ZnO/Ag bimetallic 0.1 M, 0.5 M (G) ZnO/Ag bimetallic 1 M, 1 M.

2.5. Estimation of flavonoid like property (FLP)

The estimation of Flavanoid like property of NPs was ascertained by Aluminum Chloride method [10]. 20 μl stock solutions (4 mg/ml in DMSO) was mixed with 10 μl of 10% aluminum chloride and 10 μl of 1.0 M potassium acetate in 96 well plate. 160 μl distilled water was also poured in each well. After half an hour absorbance was recorded at 415 nm. The calibration curve ($y = 0.115x + 0.141$, $R^2 = 0.996$) was drawn in accordance with the absorbance of positive control i.e. Quercetin at final concentrations 25, 12.5, 6.25 and 3.125 μg/ml under same operating conditions. The results are expressed as μg equivalents of Quercetin per milligram sample (μg QE/mg sample).

2.6. Free radical scavenging Activity-DPPH assay

To determine the antioxidant potential, 10 μl of each sample (4 mg/ ml) was treated with 190 μl of DPPH reagent (9.6 mg/ 100 ml methanol) in 96 well plate following previously published protocol [9]. The reaction mixtures were incubated for 1 h at 37 °C and absorbance was recorded at 517 nm. Ascorbic acid and DMSO were used as positive and negative control, respectively. Scavenging activity in percent (%RSA) was calculated by utilizing the equation:

Percent radical scavenging capacity = (1 – Abs / Abc) *100

Where;

Abs denotes the absorbance of DPPH solution with sample.

Abc denotes the absorbance of negative control (containing the reagent instead the sample).

2.7. Total antioxidant capacity

The estimation of the total antioxidant capacity was ascertained by Phosphomolybdenum based method [10]. A 100 μl aliquot of each sample was reacted with 900 μl of reagent (0.6 M sulphuric acid, 28 mM sodium phosphate and 4 mM ammonium molybdate). The reaction mixture was heated in water bath for 90 min at 95 °C. After the mixture cooled down absorbance was noted at 630 nm. The calibration curve ($y = 0.057x + 0.748$, $R^2 = 0.99$) was drawn in accordance with the absorbance of positive control i.e. Ascorbic acid at final concentrations 50, 25, 12.5 and 6.25 μg/ml under same operating conditions. The antioxidant activity is expressed as the number of μg equivalents of ascorbic acid per milligram sample i.e., μgAAE/mg sample.

2.8. Total reducing power determination

To determine total reducing potential of samples the method devised by Naz et al., [11] was used. From 4 mg/ml stock solution 200 μl was transferred into eppendorf tubes and was uniformly mixed with 200 μl 0.2 M phosphate buffer (pH 6.6) and 250 μl 1% potassium ferricyanide [$K_3Fe(CN)_6$]. The tubes were incubated for 20 min at 50 °C and 200 μl of 10% Trichloroacetic acid was added to each tube. The tubes were centrifuged at 300 rpm for 10 min. 150 μl of supernatant was transferred into 96 well-plate and 50 μl of 0.1% Ferric chloride was added in each well. The absorbance was recorded at 630 nm. The calibration curve ($y = 0.014x + 0.891$, $R^2 = 0.998$) was drawn in accordance with the absorbance of positive control i.e. Ascorbic acid at final concentrations of 100, 50, 25 and 12.5 μg/ml under same operating conditions. The resultant reducing power of each sample is expressed as μg AAE/mg DW.

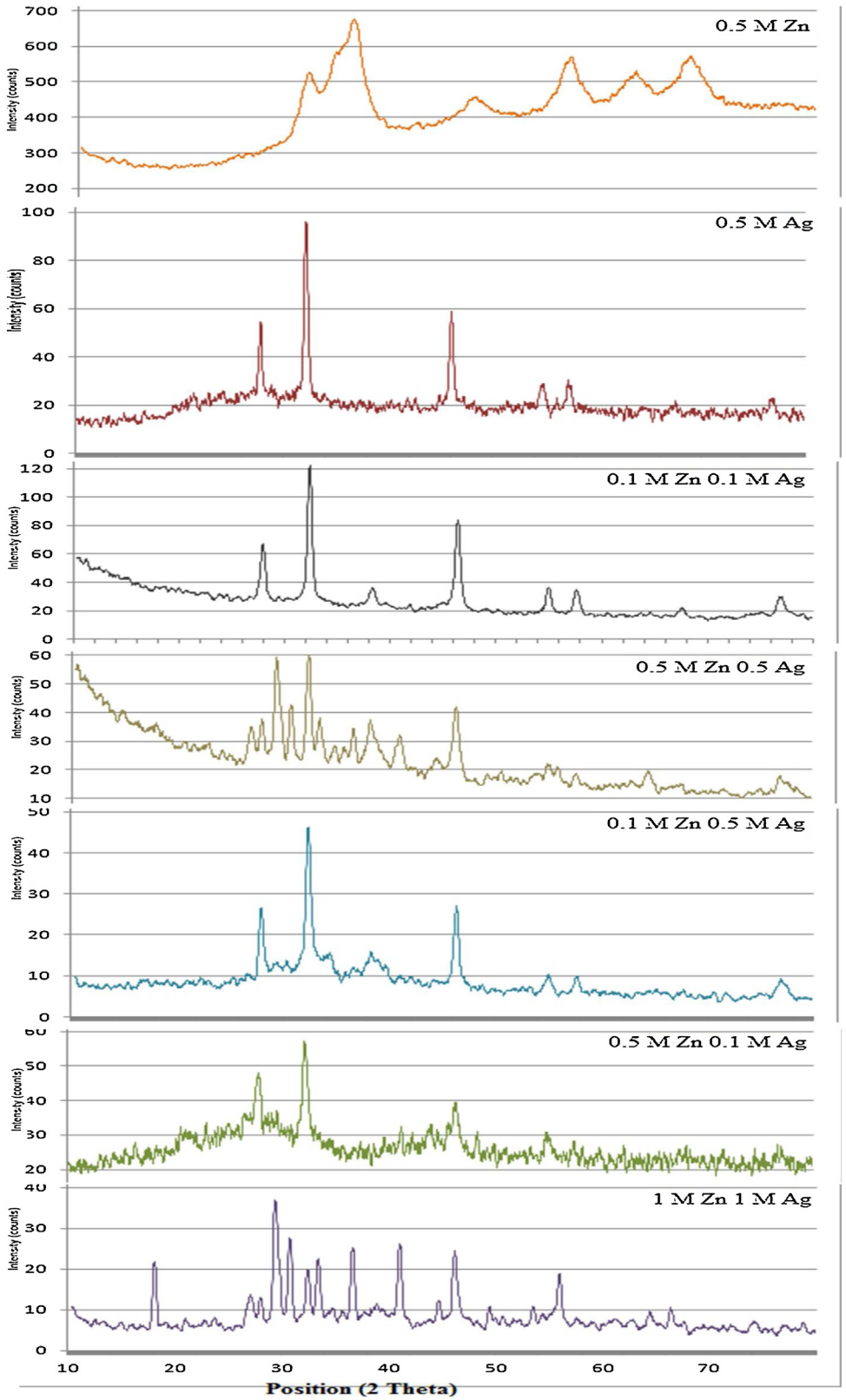

Fig. 2. XRD Patterns of monometallic and bimetallic ZnO and Ag nanoparticles.

2.9. Antibacterial assay

Antibacterial assay was performed against two Gram positive (*Staphylococcus aureus* (ATCC# 6538) and *Bacillus subtilis* (ATCC# 6633) and three Gram negative (*Escherichia coli* (ATCC 15,224), *Pseudomonas aeruginosa* (ATCC# 9721) and *Klebsiella pneumoniae* (ATCC# 4619) strains through disc diffusion method [11].

5 μl of each sample (4 mg/ml) was poured on sterile filter paper discs previously infused on the cultured plates. 5 μl of Roxithromycin and 5 μl of DMSO were poured on separate discs which

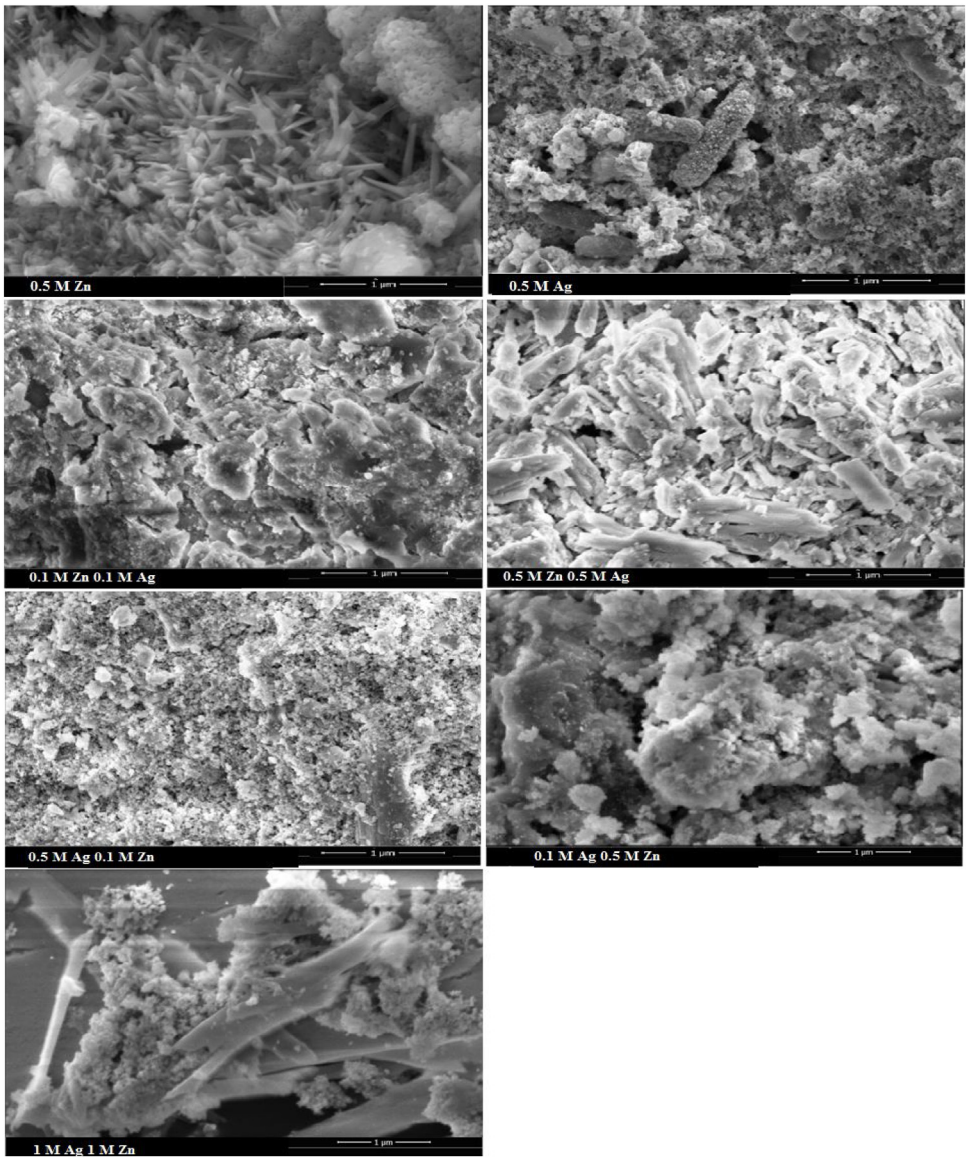

Fig. 3. SEM Images of monometallic ZnO and Ag nanoparticles and bimetallic ZnO/Ag nanoparticles.

Table 2
EDX analysis of Ag and ZnO monometallic and bimetallic NPs synthesized through green chemistry.

Sample	Zn (% weight)	Ag (% weight)
0.5Zn:0.1Ag	96.17	3.73
0.1ZnO:0.1Ag	21.34	49.21
0.5Zn:0.1Ag	81.76	13.99
0.5ZnO:0.5Ag	69.13	29.29
1ZnO:1Ag	1.1	97.4
0.5Zn	87.13	
0.5Ag	100	–

served as positive and negative controls respectively. The plates were incubated for 24 hs at 37 °C thereafter average diameter of zone of inhibition were measured.

2.10. Antileishmanial assay

Stock solutions of NPs were prepared by dispersing nanoparticles (1 mg) in 1 ml of distilled water. M199 media containing culture promastigotes were suspended to yield 1×10^6 cell/ml in each well of 96 wells plate. Afterwards, nanoparticles were added serially in each well. The final volume was attuned to 100 μl with M199 media. Control leishmanial culture was not treated with nanoparticle solution. Viability of promastigotes was analyzed by Neubauer chamber after 72 hs [9].

2.11. Statistical analysis

All the experiments were performed in triplicate. The data is presented as the mean ± Standard deviation. The results obtained were analyzed statistically for least significant difference (LSD) at $P \leq 0.05$ after analysis of variance while regression using Microsoft Excel program.

3. Results and discussion

Monometallic ZnO, Ag and bimetallic ZnO/Ag nanoparticles were synthesized by one step approach at room temperature using aqueous leaf extract of *Mirabilis jalapa* Linn. In each set of reaction, the color differed from one another depending upon salt and concentration used (Table 1, Fig. 1). The reaction mixture for ZnO

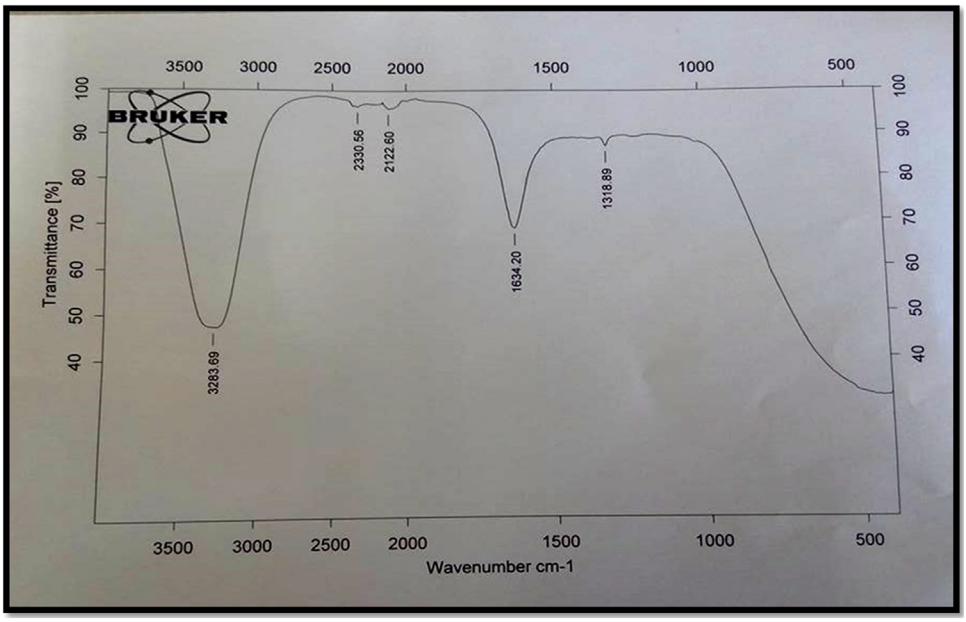

Fig. 4. FTIR Spectra of Aqueous *M. jalapa* leaves Extract.

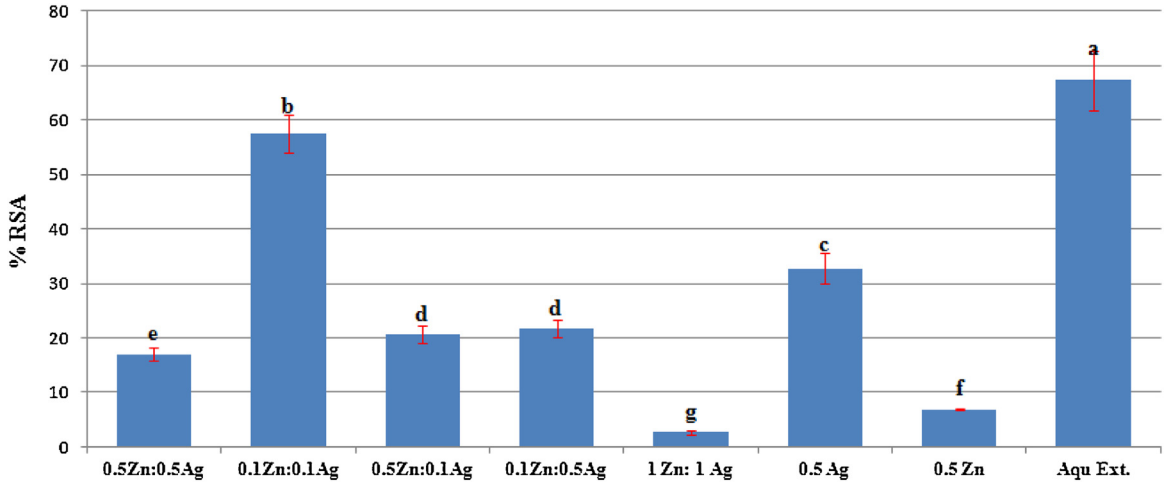

Fig. 5. Free radical scavenging activity of monometallic and bimetallic NPs.

nanoparticles exhibited light brown color while Ag NPs reaction mixture exhibited grayish black color. In case of bimetallic NPs synthesis, color of reaction mixture varied depending upon concentration and type of salt used [10,12,13]

3.1. Characterization of nanoparticles

The average size and crystallinity of nanoparticles came across by X-Ray Diffraction. The results reveal that average size of monometallic ZnO and Ag NPs was 12.9 nm and 32.8 nm, respectively. Combination of both salts in the reaction mixture resulted in change of nanoparticle size depending upon salt used (Fig. 2). It was observed that addition of silver salt at higher concentration then zinc salt decreased the size of nanoparticles. Furthermore high concentrations of both salts (1 M each) also resulted in increase in size of bimetallic NPs (Table 1). This phenomenon that silver itself or addition of Ag salt reduces the size of NPs as compared with Zn NPs alone or when incorporated into the medium has been observe by many researchers [10,14–18].

The monometallic ZnO particles presented a needle like morphology whereas the monometallic Ag nanoparticles were spherical in shape. The bimetallic combinations of Zinc oxide and Silver nanoparticles prepared at different concentrations of the precursor salts were quite different from one another like the bimetallic ZnO/Ag (0.5 M, 0.5 M) exhibited plate like structures, bimetallic ZnO/Ag (0.1 M, 0.1 M) were spherical in shape, bimetallic ZnO/Ag (0.5 M,0.1 M) displayed spherical amorphous particles, bimetallic ZnO/Ag (0.1 M,0.5 M) presented spherical structures and the bimetallic ZnO/Ag (1 M 1 M) were sheet like structures (Fig. 3). It has been reported that morphological variations of NPs depends upon type of metal, concentration of salt, physical conditions of reaction mixture, and plant extract chemistry.

The extent of purity of the monometallic and bimetallic ZnO and Ag nanoparticles was confirmed by Energy Dispersive Spectroscopy (EDAX). The EDAX profile of the bimetallic NPs at four different molarities showed strong signals for silver atoms along with comparatively weak signals from zinc, the reason behind strong silver signal is due to high reactivity of silver (Table 2). The EDAX profiles of monometallic ZnO and Ag

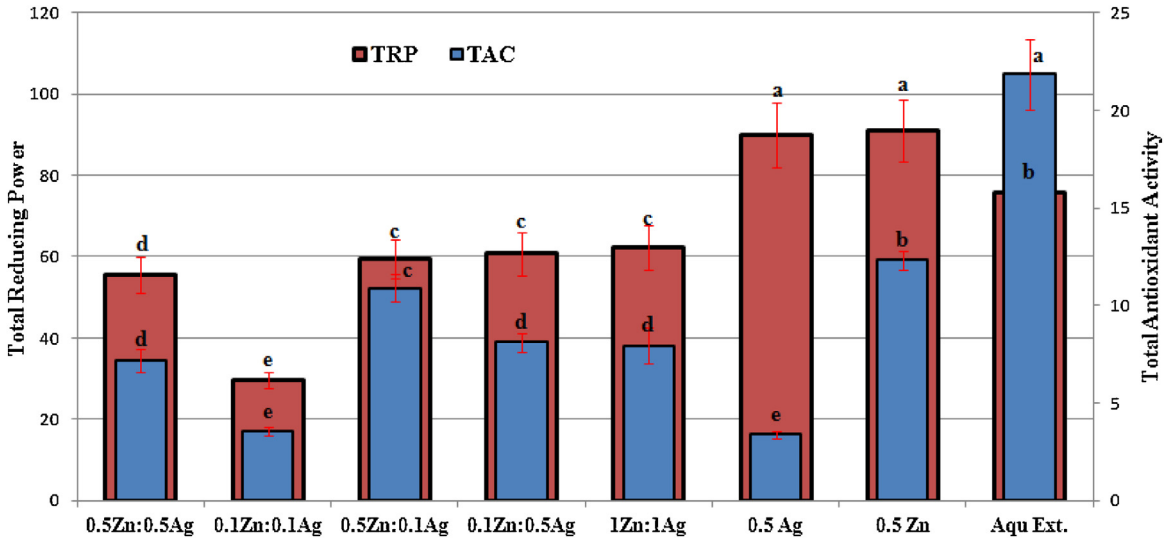

Fig. 6. Total Antioxidant capacity and Total Reducing Potential of nanoparticles and plant extract.

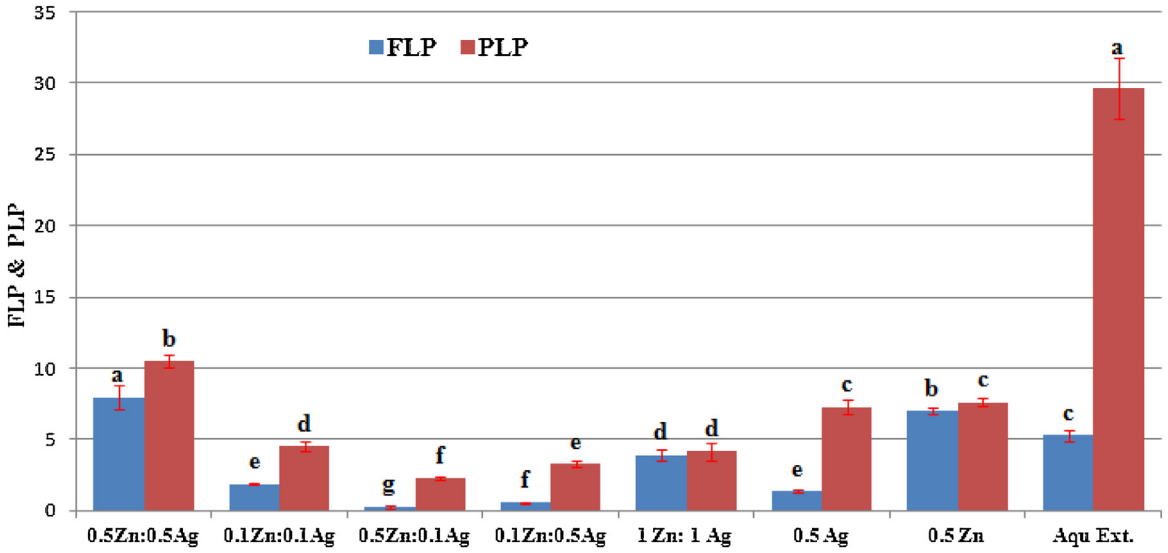

Fig. 7. Phenolic like and flavonoid like properties of nanoparticles and plant extracts.

Table 3
Diameters of the Zone of inhibition against different Bacterial Strains by samples.

Sample Name	*Pseudomonas aeruginosa*	*Klebsiella pneumonia*	*Escherichia coli*	*Staphylococcus aureus*	*Bacillus subtilis*
0.5ZnO:0.5 Ag	18 ± 1.5^{c}	25 ± 1.6^{a}	17 ± 1.5^{a}	20 ± 1.7^{b}	21 ± 1.9^{a}
0.1 ZnO, 0.1 Ag	11 ± 0.8^{f}	20 ± 1.3^{c}	16 ± 1.4^{ab}	18 ± 1.4^{c}	18 ± 1.5^{b}
0.5 ZnO, 0.1 Ag	14 ± 1.1^{d}	22 ± 1.9^{b}	12 ± 0.9^{c}	19 ± 1.5^{bc}	16 ± 1.4^{c}
0.1 ZnO, 0.5 Ag	12 ± 0.6^{e}	21 ± 1.8^{bc}	17 ± 1.5^{a}	18 ± 1.5^{c}	16 ± 1.4^{c}
0.5 ZnO	34 ± 2.6^{a}	12 ± 0.8^{d}	9.5 ± 0.5^{e}	11 ± 0.7^{d}	10 ± 0.8^{d}
0.5 Ag	15 ± 1.1^{d}	11 ± 0.7^{e}	12 ± 0.6^{d}	19 ± 1.5^{bc}	18 ± 1.6^{b}
1 ZnO: 1 Ag	21 ± 1.8^{b}	21 ± 1.8^{bc}	13 ± 0.7^{c}	22 ± 1.8^{a}	16 ± 1.3^{c}
Aqu. Extract	12 ± 0.9^{e}	11 ± 0.8^{e}	12 ± 0.9^{c}	6 ± 0.3^{e}	9 ± 0.5^{e}

nanoparticles signal of zinc and strong signals of Ag were displayed with 100% purity.

3.2. Characterization of leaf extract of M. jalapa

The FTIR spectrum of the aqueous *M. jalapa* leaves extract showed a strong and broad band at 3283.69 cm^{-1} which is the characteristic of hydroxyl group. The band at 2122.60 cm^{-1} refers to the C≡C of alkyne or CN group. The band at 1634.20 cm^{-1} can be assigned to the C=C or the N—H group. 1318.89 cm^{-1} band corresponds to C–N group of amine or C–O group of acid (Fig. 4).

In the FTIR spectrum of aqueous leaf extract of *M. jalapa* distinct IR bands correspond to alcohols, amides and amines functional groups were noticed. Comparing the presence of the –OH group

Table 4
Antileishmanial activity of monometallic and bimetallic NPs of Zn and Ag.

Conc. (μg/ml)	0.5 M:0.5 M	0.1 M,0.1 M	0.5 M,0.1 M	0.1 M,0.5 M	1 M,1 M	0.5 M ZnO	0.5 M Ag
10	11.59	30.91	5.31	10.62	1.44	5.79	5.31
5	12.56	31.88	8.69	13.04	2.41	6.76	6.76
2.5	14.00	33.33	11.59	13.52	4.34	7.24	8.21
1.25	14.97	37.19	18.35	14.97	5.79	8.69	9.66
0.625	17.39	40.57	19.80	16.425	6.76	9.17	12.56
0.3125	17.87	47.34	23.18	17.39	7.24	11.59	13.04
0.15625	18.84	49.27	23.67	18.84	14.00	13.04	14.97
0.078125	20.77	53.62	25.60	19.809	18.84	13.52	18.35

and C–O group of acid in the extracts ascertains its role in the reduction of the salts into their respective nanoparticles. Similarly, a study conducted by Vankar & Bajpai [19] reported the presence of CO groups of polyols such as flavones, terpenoids and polysaccharides in the flower extract of *M. jalapa*.

3.3. Biological assays results

The percent free radical scavenging activity (RSA) of the nanoparticles and the plant extracts was evaluated by the discoloration of DPPH reagent. The technique relies on the reduction of DPPH (Purple in Color) into stable diphenyl picrylhydrazine molecule (Yellow in Color) by accepting hydrogen radical or electron from the donor antioxidant. The Fig. 5 shows that there is variation in FRSA activity. Among the monometallic silver NPs has better capability to scavenge free radicals while in case of bimetallic NPs synthesized at low reactant concentrations has more activity (57.58% by NPs synthesized by 0.1 M Ag and Zn salt each).

The total antioxidant capacity (TAC) depends on the reduction of Mo (VI) to Mo (V) via antioxidant mediators and as a result Phosphate/Mo (V) complex (Green in Color) is formed with a maximal absorption at 695 nm. All the samples had low TAC activity irrespective to monometallic or bimetallic. TAC of NPs is less significantly different from plant extract (Fig. 6).

The total reducing potential of the nanoparticles and the plant extracts is presented in Fig. 6. The total reducing potential of ZnO/Ag BMN (1 M,1 M) was at the highest extreme by having 90.89 ± 7.6 mg AAE/g. It was observed that both monometallic ZnO and Ag NPs have greater TRP then plant extract while all bimetallic NPs except synthesized by low concentrations of salts (0.1 M each) had least TRP activity.

3.4. Phytochemical analysis

To investigate motive of free radical scavenging activity and antioxidative potential of nanoparticles, phenolic and flavonoid like potential of nanoparticals was also investigated (Fig. 7). The nanoparticles showed different behavior in response to reaction mixtures for phenolics and flavonoids. Bimetallic NPs synthesized by 0.5 M zinc and silver salts have significant activity then others. These activities are most presumably due to presence of different functional groups on the surface of nanoparticles. Zinc and silver ions released from the NPs might also be involved in these activities.

3.5. Antibacterial assay

Comparing the antibacterial activity of the nanoparticles and plant extracts, the activity of nanoparticles dominate the activity of plant extracts. Among the nanoparticles the BMN were more potent antibacterials as compared to their MMN counterparts (Table 3). The maximum zone of inhibition was produced by ZnO/Ag BMN (0.5 M, 0.5 M) against *Klebsiella pneumonia* with a diameter of 25 ± 1.6 mm. While 22 ± 1.8 mm inhibition zone against *Staphylococcus aureus* was shown by ZnO/Ag (1:1 M). ZnO monometallic nanoparticles produced 34 mm zone against *Pseudomonas aeruginosa* that was not purely a clearing zone instead a retarding zone. It has been reported that Silver is antibacterial agent while zinc kills the bacterial due to activation of electrons and also the ions of both have antibacterial potential. Therefore bimetallic NPs have better activities even synthesized through different processes [20–22]. The difference in antibacterial by monometallic and bimetallic nanoparticles can be drawn by different ways. First the physiological, morphological and biochemical of the strains that mainly differ between Gram positive and Gram negative strains. Secondly the morphology and other physiological characteristics of nanoparticles. Smaller nanoparticles may invade inside the cell and cause toxicity effects. Third and most important the ion released in the medium from nanoparticles have lethal effect on microbial cells. These released ions and nanoparticles itself inside the cell may react with biomolecules causing death of cell. Such mechanisms have been explained by many researchers [23–26].

3.6. Antileishmanial assay

Upon the investigation of the antileishmanial potential of the nanoparticles and plant extract, only the nanoparticles showed the potency to kill the parasite. ZnO/Ag BMN (1 M, 1 M) among all other samples showed the highest potency to kill the parasite (Leishmania) (Table 4). A study reported the antileishmanial activity of silver nanoparticles synthesized via *Sargentodoxa cuneata* by Ahmad et al, [27] as well as antileishmanial activity of ZnO nanoparticles synthesized via *Linum usitatissimum L* [28], comparing the activity of the bimetallic nanoparticles with monometallic nanoparticles. It is apparent that the activity of bimetallic is greater than monometallic, the higher the concentration of the nanoparticles the greater is the activity [29]. The synergistic effect of both metals (Zn and Ag) in for of nanoparticles or released ions has prognostic effect of antibacterial, antileishmanial and other biological activities.

4. Conclusion

The utilization of plant extracts for nanoparticle synthesis suggests a lot of benefits over chemical methods like their environment friendliness and cohesiveness for pharmaceutical and various biomedical uses because of the omission of the usage of toxic compounds. In the context of bimetallic nanoparticles, the results provide strong evidence that could warrant the consideration of ZnO/Ag Bimetallic nanoparticles as antimicrobial agents that could circumvent the side and passive immune effects of other biocidal medications. Moreover the bimetallic nanoparticles are more reactive due to synergistic effect of both metals. It can also be supposed that the bimetallic nanoparticles has different intensity

of configuration, strength, binding and interaction that make them more reactive. Prior to the commercialization of the Nanoantibiotics, these require a lot of thorough attention in order to take full advantage of these miraculous agents.

Conflict of interest

Authors declare no conflict of interest.

References

[1] A. Zaleska-Medynska, M. Marchelek, M. Diak, E. Grabowska, Noble metal-based bimetallic nanoparticles: the effect of the structure on the optical, catalytic and photo catalytic properties, Adv. Colloid Interface Sci. 229 (2016) 80–107.

[2] M. Vaseem, A. Umar, Y.B. Hahn, ZnO nanoparticles: growth, properties, and applications, Metal Oxide Nanostructures and Their Applications, vol. 5(2010), pp. 1–36.

[3] D. Nohavica, P. Gladkov, ZnO nanoparticles and their applications-new achievements, Olomouc, Czech Republic, EU 10 (2010) 12–14.

[4] K.I. Bogutska, Y.P. Sklyarov, Y.I. Prylutskyy, Zinc and zinc nanoparticles: biological role and application in biomedicine, Ukrainica Bioorganica Acta 1 (2013) 9–16.

[5] P.K. Biswas, S. Dey, Effects and applications of silver nanoparticles in different fields, Int. J. Recent Sci. Res. 6 (8) (2015) 5880–5883.

[6] P. Fageria, S. Gangopadhyay, S. Pande, Synthesis of ZnO/Au and ZnO/Ag nanoparticles and their photo catalytic application using UV and visible light, R. Soc. Chem. Adv. 4 (48) (2014) 24962–24972.

[7] Y. Zheng, L. Zheng, Y. Zhan, X. Lin, Q. Zheng, K. Wei, Ag/ZnO heterostructure nanocrystals: synthesis, characterization, and photo catalysis, Inorg. Chem. 46 (17) (2007) 6980–6986.

[8] H.R. Liu, G.X. Shao, J.F. Zhao, Z.X. Zhang, Y. Zhang, J. Liang, B.S. Xu, Worm-like Ag/ZnO core–shell heterostructural composites: fabrication, characterization, and photocatalysis, J. Phys. Chem. C 116 (30) (2012) 16182–16190.

[9] R. Javed, M. Ahmed, I. ul Haq, S. Nisa, M. Zia, PVP and PEG doped CuO nanoparticles are more biologically active: Antibacterial, antioxidant, antidiabetic and cytotoxic perspective, Mater. Sci. Eng. C 79 (2017) 108–115.

[10] M. Zia, S. Gul, J. Akhtar, I. Ul Haq, B.H. Abbasi, A. Hussain, M.F. Chaudhary, Green synthesis of silver nanoparticles from grape and tomato juices and evaluation of biological activities, IET Nanobiotechnol. 11 (2) (2016) 193–199.

[11] S. Naz, S. Tabassum, N. Freitas Fernandes, M. Mujahid, M. Zia, E.J. Carcache de Blanco, Anticancer and antibacterial potential of Rhus punjabensis and CuO nanoparticles, Nat. Prod. Res. (2018) 1–6.

[12] P. Sutradhar, M. Saha, Green synthesis of zinc oxide nanoparticles using tomato (Lycopersicon esculentum) extract and its photovoltaic application, J. Exp. Nanosci. 11 (5) (2016) 314–327.

[13] A.M. Awwad, N.M. Salem, Green Synthesis of Silver Nanoparticles byMulberry LeavesExtract, Nanosci. Nanotechnol. 2 (4) (2012) 125–128.

[14] A. Ali, S. Ambreen, R. Javed, S. Tabassum, I. ul Haq, M. Zia, ZnO nanostructure fabrication in different solvents transforms physio-chemical, biological and photodegradable properties, Mater. Sci. Eng. C 74 (2017) 137–145.

[15] H. Gebru, A. Taddesse, J. Kaushal, O.P. Yadav, Green synthesis of silver nanoparticles and their antibacterial activity, J. Surf. Sci. Technol. 29 (2013) 47–66.

[16] C. Dwivedi, V. Dutta, Size controlled synthesis of ZnO nanoparticles via electric field assisted continuous spray pyrolysis (EACoSP) reactor, Appl. Phys. A 109 (1) (2012) 75–79.

[17] M. Naushad, Surfactant assisted nano-composite cation exchanger: development, characterization and applications for the removal of toxic Pb2+ from aqueous medium, Chem. Eng. J. 235 (2014) 100–108.

[18] M. Naushad, A. Mittal, M. Rathore, V. Gupta, Ion-exchange kinetic studies for Cd (II), Co (II), Cu (II), and Pb (II) metal ions over a composite cation exchanger, Desalin. Water Treat. 54 (10) (2015) 2883–2890.

[19] P.S. Vankar, D. Bajpai, Preparation of gold nanoparticles from *Mirabilis jalapa* flowers, Indian J. Biochem. Biophys. 47 (3) (2010) 157–160.

[20] W. Lu, G. Liu, S. Gao, S. Xing, J. Wang, Tyrosine-assisted preparation of Ag/ZnO nanocomposites with enhanced photocatalytic performance and synergistic antibacterial activities, Nanotechnology 19 (44) (2008) 445711.

[21] H. Koga, T. Kitaoka, H. Wariishi, In situ synthesis of silver nanoparticles on zinc oxide whiskers incorporated in a paper matrix for antibacterial applications, J. Mater. Chem. 19 (15) (2009) 2135–2140.

[22] S. Ghosh, V.S. Goudar, K.G. Padmalekha, S.V. Bhat, S.S. Indi, H.N. Vasan, ZnO/Ag nanohybrid: synthesis, characterization, synergistic antibacterial activity and its mechanism, R. Soc.Chem. Adv. 2 (3) (2012) 930–940.

[23] G. Sharma, D. Pathania, M. Naushad, N.C. Kothiyal, Fabrication, characterization and antimicrobial activity of polyaniline Th (IV) tungstomolybdophosphate nanocomposite material: efficient removal of toxic metal ions from water, Chem. Eng. J. 251 (2014) 413–421.

[24] S.M. Alshehri, M. Naushad, T. Ahamad, Z.A. Alothman, A. Aldalbahi, Synthesis, characterization of curcumin based ecofriendly antimicrobial bio-adsorbent for the removal of phenol from aqueous medium, Chem. Eng. J. 254 (2014) 181–189.

[25] D. Pathania, G. Sharma, M. Naushad, A. Kumar, Synthesis and characterization of a new nanocomposite cation exchanger polyacrylamide Ce (IV) silicophosphate: photocatalytic and antimicrobial applications, J. Ind. Eng. Chem. 20 (5) (2014) 3596–3603.

[26] R. Katwal, H. Kaur, G. Sharma, M. Naushad, D. Pathania, Electrochemical synthesized copper oxide nanoparticles for enhanced photocatalytic and antimicrobial activity, J. Ind. Eng. Chem. 31 (2015) 173–184.

[27] A. Ahmad, F. Syed, A. Shah, Z. Khan, K. Tahir, A.U. Khan, Q. Yuan, Silver and gold nanoparticles from *Sargentodoxa cuneata*: synthesis, characterization and antileishmanial Activity, R. Soc. Chem. Adv. 5 (90) (2015) 73793–73806.

[28] B.H. Abbasi, S. Anjum, C. Hano, Differential effects of in vitro cultures of *Linum usitatissimum* L. (Flax) on biosynthesis, stability, antibacterial and antileishmanial activities of zinc oxide nanoparticles: a mechanistic approach, RSC Adv. 7 (26) (2017) 15931–15943.

[29] A. Ali, A.R. Phull, M. Zia, Elemental Zinc to Zinc nanoparticles: Is ZnO NPs crucial for life? Synthesis, toxicological and environmental concerns, Nanotechnol. Rev. 7 (5) (2018) 413–441.